

SUPPLEMENTARY MATERIALS

Figures

Fig. S1. Generation of EPAC1-null mice.

Fig. S2. Vascular integrity assessments.

Fig. S3. Normal rabbit serum was used as an antibody control for immunohistochemistry and immunofluorescence staining.

Fig. S4. Comparison of clotting parameters and other components of the fibrinolytic system.

Fig. S5. Histological observation of FeCl₃-induced carotid arterial thrombosis.

Fig. S6. Absence or inhibition of EPAC1 does not affect *de novo* protein synthesis of ANXA2 and S100A10.

Fig. S7. Lipid raft fraction-associated monosialotetrahexosyl ganglioside assay and non-lipid raft fraction-associated immunoblotting with anti-transferrin receptor.

Fig. S8. Inhibition of EPAC1 does not affect the levels of other plasminogen receptors.

Materials and Methods

Clinical biopsy samples

In four cases of rheumatic mitral stenosis with chronic atrial fibrillation, left atrial mural thrombi were seen in the left atrial appendages during open heart surgeries for mitral valve replacements under extracorporeal circulation support at Changhai Hospital, the Second Military Medical University (Shanghai, China). After removing the thrombus, a 5 x 5 mm² piece of endocardial tissue (including cardiac endothelium) directly underneath the thrombus in the left atrial appendage was harvested. Tissue samples were flash frozen in liquid nitrogen and homogenized for immunoblotting assays by pulverizer (Spectrum Laboratories, Rancho Dominguez, CA) as described previously¹. The biopsy incision was closed with a 5-0 polypropylene suture. Similar tissue samples from normal donor hearts were used as normal controls. Informed written consent was obtained from each patient prior to study enrollment. This study was approved by the Committee on Ethics of Changhai Hospital, Shanghai, China (SMMUEC 2015-46) and abided by the Declaration of Helsinki principles.

Mice

All procedures on animals were performed in accordance with approval of the Scientific Investigation Board of Changhai Hospital, the Second Military Medical University, Shanghai, China or the UTMB Institutional Animal Care and Use Committee. All mice used in this study were 7- to 10-weeks-old. Equal numbers of males and females were used.

To ascertain the role of EPAC1 *in vivo*, we generated *KO* mice that carry the *Rapgef3* (also known as *EPAC1*) allele lacking exons 3-6. We confirmed that the mutant allele is null by Western immunoblotting analysis (WB) (**Fig. S1**). Similar to published models^{2,3}, our *KO* mice are viable, fertile, and without overt abnormalities.

EPAC1 mutant mice carrying a conditional-ready allele (B6;129S2-*Rapgef3*^{tm1Geno}/J, the Jackson Laboratory, Stock No. 018389) were obtained, and crossed with a germline Cre deletion mouse, C57BL/6-Tg(Zp3-cre)93Kw/J (The Jackson Laboratory, Stock No. 003651), to generate knockout mice. The majority of the mice used in experiments (homozygotes and wild-type controls) were C57BL/6J incipient congenic (N5), and generated by heterozygous intercrosses.

Epac-specific inhibitor ESI09 treatment of wild-type mice by the intraperitoneal route was described previously⁴. Briefly, twelve C57BL/6J mice were divided into two groups. Six mice were treated with ESI09 (10 mg/kg/day dissolved in buffered saline containing 10% ethanol and 10% Tween-80) via intraperitoneal injection for five days before euthanasia. The other six animals were treated with vehicle. One minute following euthanasia, 5 mL of cold saline solution was injected into the intra-left ventricle in preparation for tissue collection. An extensive *in vivo* perfusion of the animal prior to collection of fibrin-relevant tissue has been described⁵.

Antibodies and other reagents

Anti-annexin A2 (ANXA2) mouse monoclonal antibody (mAb) (clone 5) and rabbit polyclonal antibodies (clone H50) were purchased from BD Biosciences (San Jose, CA) and Santa Cruz Biotechnology (Dallas, TX), respectively. Anti-tyrosine 23 phosphorylated annexin A2 mAb (clone 11.Tyr24) and anti-enolase mAb antibodies were purchased from Santa Cruz Biotechnology. Anti-S100A10 (S100A10) mAb (clone 4E7E10) and goat polyclonal antibodies (product AF2377) were purchased from Thermo Fisher Scientific (Rockford, IL) and R&D Systems (Minneapolis, MN), respectively. Anti-EPAC1 mAb (clone 5D3) and rabbit polyclonal antibody were purchased from Cell Signaling

Technology (Danvers, MA) and Thermo Fisher Scientific, respectively. Anti-fibrin mAb was purchased from Creative Diagnostics (DMABT-Z59493, Shirley, NY). Anti-fibrin(ogen) rabbit polyclonal antibody was purchased from DAKO (Carpinteria, CA)⁵. Anti- α -tubulin mAb (clone B-7) was purchased from Santa Cruz Biotechnology. Anti-human Na⁺-K⁺ ATPase β 3 mAb (Clone 46) was purchased from BD Bioscience (San Jose, CA). Anti-transferrin receptor mAb (H68.4), anti-cytokeratin-8, and anti GAPDH mAb (6C5) was purchased from Thermo Fisher Scientific. Anti VE-cadherin mAb was purchased from Meridian Life Science (Saco, ME). Anti-plasminogen receptor-KT rabbit polyclonal antibody was purchased from EpiGentek (Farmingdale, NY). Anti-von Willebrand factor (vWF), anti-ZO-1 and anti-occludin rabbit polyclonal antibodies were purchased from Thermo Fisher Scientific. Src family activator phosphopeptide⁶ was purchased from Santa Cruz Biotechnology. Recombinant cholera toxin subunit-horseradish peroxidase conjugate (CTB-HRP) from Sigma Aldrich (St. Louis, MO) was used. Anti-PIP2 mAb was purchased from (Novus Biologicals, Littleton, CO). The phospholipid assay kit was purchased from Thermo Fisher Scientific. AlexaFluor 488-conjugated goat anti-mouse and ProLong Gold Antifade Reagent with DAPI were purchased from Invitrogen (Carlsbad, CA). Horseradish peroxidase-conjugated (HRP-) goat anti-mouse IgG and horseradish peroxidase-conjugated goat anti-rabbit IgG were purchased from Southern Biotech (Birmingham, AL). HRP-goat anti-mouse IgG and IgM (H+L) was purchased from Thermo Fisher Scientific. Unless otherwise indicated, all reagents were purchased from Thermo Fisher Scientific.

Carotid artery thrombosis model

Mice were subjected to carotid artery injury using FeCl₃ as described previously⁷⁻¹⁰. In brief, C57BL/6 mice were anesthetized with 1%-4% isoflurane inhalation. The left carotid artery of the mouse was exposed and a miniature ultrasound flow probe (0.5VB; Transonic System, Ithaca, NY) was placed around the vessel. Baseline artery blood flow was recorded every minute for five minutes using a Transonic T201 two-channel ultrasonic blood flow meter (Transonic System, Ithaca, New York, USA). To induce arterial thrombosis injury, a 1 x 1-mm filter paper soaked with 7.5% ferric chloride (FeCl₃) was applied to the adventitial surface of the artery for three minutes. Following removal of the filter paper, carotid blood

flow recording was resumed for 30 minutes, and complete thrombotic occlusion was defined when flow decreased to and stayed at 0 ml/min for 1 minute ⁷. In recombinant ANXA2 (rANXA2) (a N-Terminal His-tag and corresponding to the amino acids 1-339 of Human ANXA2) reintroduction experiments, after baseline flow was recorded the animals were injected intravenously with rANXA2 (Novus Biologicals) at 2 mg/kg⁸ or the same dose of bovine serum albumin (BSA); blood flow was recorded for another 10 minutes before FeCl₃ was applied. After euthanasia, 30 mL of cold phosphate-buffered saline (PBS) was injected into the left ventricle at 3mL/min. The cervical organs were removed *en bloc* and immersion-fixed in 10% neutral-buffered formalin for histological analysis. Near-serial cross sections were stained with the use of hematoxylin and eosin to detect thrombus in carotid arteries by bright field microscopy ¹¹.

Cell culture

Human umbilical vein endothelial cells (HUVECs) (Cell Applications, Atlanta, GA) were grown in Endothelial Cell Growth Medium (Cell Applications, Atlanta, GA) supplemented with 10% heat-inactivated fetal bovine serum (FBS) with humidity in 5% CO₂ at 37°C. The media was changed every 48 h. Cells were allowed to grow 48 h until 90% confluence of the monolayer was achieved. Cells were maintained in Endothelial Cell Growth Medium during the experiments. Cell passages 2–5 were used for all experiments.

EPAC-specific inhibitor (ESI09) was purchased from Tocris Bioscience (Avonmouth, Bristol, United Kingdom). For *in vitro* studies, HUVECs were exposed to 5 µmol/L EIS09 in medium for 24 h. Medium with 0.01 % dimethyl sulfoxide (vol/vol) was used as vehicle control. In stimulation experiments, HUVECs were starved using Endothelial Basic Medium (Cell Applications) with 0.1% FBS for 2 h followed by stimulation with serum or Src family activator phosphopeptide (10 µmol/L) ^{6,12} for 15 minutes before fixation or cell membrane fractionation.

For ectopic expression of ANXA2, HUVECs were grown in 12-well tissue culture plates until 90% confluence of the monolayer was achieved. Transfection with pEGFP-HA vector expressing full-length ANXA2-GFP fusion protein (ANXA2-GFP) (University of Dundee, Dundee, UK) was performed using Targefect F2 reagent and Peptide enhancer (Targeting Systems, El Cajon ,CA) one day before treatment with ESI09 or Vehicle. An empty pEGFP-HA vector was

included as a negative control. After 48 h, GFP expression was confirmed by fluorescence microscopy. For the rescue experiment, transfection with pEGFP-HA vectors expressing phospho-(Tyrosine)-mimetic of ANXA2-GFP fusion protein (ANXA2 Y23E-GFP, University of Dundee, Dundee, UK) was performed using Targefect F2 reagent and Peptide enhancer (Targeting Systems, CA) one day before treatment with ESI-09 or Vehicle. An empty pEGFP-HA vector was included as a negative control. After 48 h post-transfection (p.t.), GFP expression was confirmed by fluorescence microscopy.

Hematology tests

Plasma samples from citrated blood collected from wild-type and *EPAC1*-null mice were used for the prothrombin time (PT), activated partial thromboplastin time (aPTT), and clot lysis assay¹³. Thromboplastin-D and aPTT-XL (Ellagic Acid Activator) with CaCl₂ were purchased from Thermo Fisher Scientific (Rockford, IL). The PT and aPTT were determined following the manufacturer's instructions. In brief, the PT was determined by adding Thromboplastin-D to plasma samples. The time was measured immediately until clot formation. The aPTT was determined by adding aPTT-XL and CaCl₂ into plasma samples. The time was measured immediately until clot formation. Euglobulin precipitates were prepared by adding 0.02% acetic acid into plasma (final PH 5.5) for clot lysis assay¹⁴. This mixture was kept at 8°C for 10 min, followed by centrifugation at 2,000 x g for 10 min. Euglobulin precipitates were resuspended in borate buffer (pH 8.8) in a 37° water bath for 10 min, and then clotted with an equal volume of 0.05mol/L CaCl₂. The clots were examined every 15 min. The time for total lysis of the clot was recorded as clot lysis time.

Platelets were counted manually under a microscope using an Improved Neubauer hemocytometer. Blood was diluted 1:20 with saline. The number of platelets per liter of blood was then calculated.

Wild-type and *EPAC1*-null mice were anesthetized with isoflurane. The bottom 3 mm of the tail was clipped off with a scalpel. The bleeding tail was placed in 37°C saline. The time until bleeding stopped was recorded as the bleeding time¹⁵.

Endothelial cell membrane fractionation, immunoprecipitation (IP), and immunoblotting assays

To obtain endothelial cell membrane fractions for Western immunoblotting/IP, at the end of designed experiments cells were collected and incubated in hypotonic fractionation buffer (250 mmol/LM sucrose, 20 mmol/L 4-[2-hydroxyethyl]-1-piperazineethanesulfonic acid, 10 mmol/L KCl, 1.5 mmol/L MgCl₂, 1 mmol/L ethylene diamine tetra-acetic acid, 1 mmol/L ethylene glycol tetraacetic acid, 1 mmol/L dithiothreitol, pH 7.4) supplemented with Protease Inhibitor Cocktail (Abcam, Cambridge, MA) for 20 min on ice prior to passing through a 25 G needle (Thermo Fisher Scientific). After removal of the cell nuclei by centrifugation at 720 x g for 5 min, the supernatant (post-nuclear fraction) was centrifuged at 10,000 x g for 10 min. The supernatant was collected and further centrifuged at 100,000 x g for 1 hr. The pellet was collected as the cellular membrane fraction.

For the IP study, equal amounts of soluble proteins were mixed with Dynabead Protein G (Invitrogen) conjugated with anti-S100A10 antibody, and were incubated for 24 h at 4° C. The Dynabead-antibody-antigen complex pellets were precipitated and separated using DynaMag-2 (Invitrogen). Samples were then separated by gel electrophoresis followed by immunoblotting. All experiments were repeated three times.

For immunoblotting assays, equal amounts of soluble protein were subjected to 12% SDS–polyacrylamide gel electrophoresis (SDS-PAGE). Proteins were transferred onto a polyvinylidene difluoride membrane and then incubated with primary antibody (1:1,000 for anti- Epac1, fibrin, ANXA2, S100A10, Na⁺-K⁺ ATPase, and α -tubulin antibodies; 1:500 for anti-Tyr23-ph-ANXA2 mAb), followed by incubation with a secondary antibody at 1:2,000 for 1 hr. A goat anti-mouse IgG and IgM (H+L)-HRP (Thermo Fisher Scientific) was used as the secondary antibody for the anti-fibrin mAb. Blots were visualized using an enhanced chemiluminescence kit (LI-COR Biosciences, Lincoln, NE). For quantification, fibrin standard prepared as reported ⁷. All experiments were repeated three times.

Immunohistochemistry (IHC), immunofluorescence (IF), impermeable cell-based enzyme-linked immunosorbent (ELISA), and ELISA assay.

Tissues collected from wild-type and *EPAC1*–null animals after extensive perfusion *in vivo* were fixed in 4% neutral buffered formaldehyde, embedded in paraffin, sectioned at 5 μ m thickness, and processed by hematoxylin and eosin (H&E)

staining for histopathologic evaluation and by IHC. For IHC studies on mouse tissues, deparaffinized and rehydrated sections were blocked with Ultra V Block (Thermo Fisher Scientific) for 10 minutes at room temperature before incubation with rabbit polyclonal antibody against fibrin(ogen) (DAKO) (1:500) overnight at 4°C. Normal rabbit serum (DAK) was used as a negative control. Biotinylated goat anti-rabbit IgG(H+L) (Vector Laboratories, Burlingame, CA) was employed as the secondary antibody. Specific antibody binding was detected by color detection using the 3,3-diaminobenzidine tetrahydrochloride (DAB) reaction. For IF studies, including dual-target IF staining of EPAC1 and fibrin(ogen) on archival clinical endocardial samples or tissues from experimental animals, deparaffinized and rehydrated sections were incubated with rabbit polyclonal anti-ZO-1 (1:500), anti-occludin (1:500), and anti-fibrin(ogen) antibodies, and anti-EPAC1 (dilution, 1:500) mAb (1:500) overnight at 4°C. Epac1 and fibrin/ZO-1/occludin were detected with AlexaFluor 594 goat anti-mouse and AlexaFluor 488 goat anti-rabbit antibodies. Nuclei were counterstained with DAPI. Normal mouse IgG (Vector Laboratories) or normal rabbit serum was used as a negative control. For dual-target IF staining of vWF and fibrin(ogen) in mouse tissues collected after *in vivo* extensive perfusion, Ultra V Block and normal rabbit serum were employed for the reduction of nonspecific background before and after vWF antigen-labeling, respectively. Deparaffinized and rehydrated sections of 5 µm thickness were incubated with anti-vWF rabbit polyclonal antibody (1:100) for 2 h at 21°C, followed by AlexaFluor 488-conjugated goat anti-rabbit IgG (1:1000) (Invitrogen) for 30 minutes at 21°C. The fibrin(ogen) antigens in tissues were visualized afterward by incubation with DyLight 594 Microscale Antibody Labeling Kit (Thermo Fisher Scientific) labeled anti-fibrin(ogen) rabbit polyclonal antibody (1:100 for brain; 1:500 for lung and kidney) for 2 h at 21°C. Nuclei were counter-stained with DAPI. Fluorescent images were analyzed using an Olympus BX51 epifluorescence or Nikon Eclipse Ti confocal microscope.

For the impermeable cell-based ELISA assay^{16,17}, HUVECs were cultivated on type 1 rat-tail collagen-coated 96-well plates until 90% confluence was obtained. The cells were washed at least three times in PBS before the cells were fixed with 4% paraformaldehyde for 24 hrs. Non-permeabilized fixed cells were processed according to IF protocols as described previously⁴ using anti-ANXA2 mAb (1:500) and anti-S100A10 mAbs (1:500), anti-enolase (1:500), anti-PLGRKT (1:500),

and anti-cytokeratin 8 (1:500) antibodies. Normal mouse IgG or normal rabbit serum was used as a negative control. The cells were incubated with AlexaFluor 488 goat anti-mouse for 1 hr. The reactions were read in a Thermo Fluoroskan microplate reader at single excitation (488 nm) wavelengths. Subsequently, the cellular protein was stained with sulforhodamine B (Thermo Fisher Scientific) in order to obtain an estimate for cell number. Stained HUVECs were permeabilized in 0.1% Triton X-100 in PBS before reincubation with sulforhodamine B. The reactions were read at the 550nm wavelength. Cell surface protein values are expressed as fluorescence units normalized to cell protein (FU/A550). All experiments were performed in triplicate.

Plasma samples from citrated blood collected from wild-type and *EPAC1*-null mice were used for ELISA to detect components of the fibrinolytic system¹⁸, including vWF (abcam), fibrinogen (Thermo Fisher Scientific), plasminogen (Aviva Systems Biology, San Diego, CA), D-dimer (Cloud-clone, Katy, TX), tissue plasminogen activator (tPA) (MyBioSource, San Diego, CA), and PAI-1 (R&D Systems). Standard curves were created by serial dilution of standard proteins provided in the ELISA kits. All ELISA plates were read at 450nm according to the manufacturer's directions.

Atomic force microscopy (AFM)

AFM is an advanced tool for studying biomechanical properties and has been used to determine the expression levels of cell surface proteins by measuring the binding affinity of specific protein-protein interactions, including antigen-antibody and receptor-ligand, with nanoforce spectroscopy^{19,20}. In our study, anti-ANXA2 or P11 antibodies were immobilized on polystyrene spheres attached to a colloidal cantilever. We measured the specific unbinding force during rupture of the interaction between the antigen (ANXA2 or P11) expressed in designated fields at the apical surface of living HUVECs and the antibody-coated AFM cantilever probe. Interactions between antibodies on the AFM cantilever and cell surface antigens cause large adhesion forces, which are quantified by the deflection signal during separation of the cantilever from the cell. By tracking the cantilever deflection and retraction cycle, the binding, stretching, and ruptures of antibody-antigen complexes can be monitored in terms of the adhesive force changes on the cantilever over the distance traveled by the cantilever. Representative force-distance (FD) curves exhibit rupture events occurring during the interaction between

antigens and antibodies in designated fields on the surface of a single living HUVEC (**Fig. 5B**). Therefore, by integrating the areas underneath the FD curve and above the baseline (zero force in **Fig. 5B**), we calculated the work that is required to break all interactive bonds between the cantilever and the EC, reflecting the quantity of antigen expression on the surface^{19,20}. The biomechanical properties of ANXA2 and S100A10 at the cell surface were studied using an AFM system (Flex-AFM, Nanosurf AG, Liestal, Switzerland) that utilized relevant antibody-functionalized AFM probes. Colloidal cantilevers with a 5 μm polystyrene bead were used (SHOCON-G-PS, Applied NanoStructures, Mountain View, CA) to measure surface protein interaction forces^{20,21}. The cantilevers were functionalized by incubation with anti-ANXA2 mAb or anti-S100A10 mAb at 100 $\mu\text{g/ml}$ in 0.1 M NaHCO_3 (pH 8.6) overnight at 4°C. Unbound proteins were rinsed off using PBS. The exposed surface of the bead was blocked by BSA (Sigma, St. Louis, MO) at 500 $\mu\text{g/ml}$ in PBS²⁰. AFM imaging and measurements were generally taken within 1 h after blocking. The spring constant of the cantilever was calibrated using the Sader method in air²². The cantilever spring constant varied between 0.10-0.15 N/m. Force spectroscopy was done in static force mode operating on 25 μm^2 areas on a living cell surface. The functionalized cantilever was manipulated into contact with the surface of a confluent monolayer of HUVECs. The maximum compression force was set to 150 pN. The contact time was kept constantly at 500 msec before the cantilever was retracted at a constant pulling speed of 1 $\mu\text{m/s}$ to measure the force-extension curve. In order to evaluate the effect of nonspecific unbinding force, confluent cell monolayers were pretreated with ANXA2 or S100A10 antibodies at 25 $\mu\text{g/ml}$ for 30 min to block ANXA2 or S100A10 on the cell surface before the AFM measurements. We scanned five cells per group, each with a different cantilever. Force-distance curves were analyzed using the open source software Atomic J²³.

Cell-based plasminogen binding and plasminogen activation assays^{24,25}

Preparation of FITC Glu-Plasminogen (Haematologic Technologies, Essex Junction, VT) has been described²⁵. Vehicle- or ESI09-treated HUVECs were washed, trypsinized and cultured in the absence of serum for 2 hours before incubation with 200nM FITC Glu-plasminogen, with or without ϵ -ACA (100 mmol/L) for 1 h at 4°C. Plasminogen binding was measured using a fluorescence-activated cell sorter (FACS). For carboxypeptidase B (CpB) treatment, cells were

incubated for 20 minutes at 37°C in the presence of 5 U/mL CpB. Both ϵ -ACA and CpB are used as an assay control.

Plasminogen activation was assessed by determining plasmin generation by HUVECs using both cells in confluent monolayers (ELLIS) and in suspension^{24,25}. For measuring in suspension, vehicle- or ESI09 (5 μ mol/L)-treated HUVECs were trypsinized and washed before the same procedures for confluent monolayers were used. Vehicle- or ESI09-treated HUVECs in monolayers were washed and cultured in the presence of tPA (5 nmol/L) for 20 min at 4°C before incubation with 0.5 μ mol/L Glu-plasminogen and 250 μ mol/L plasmin substrate S2251 (Diapharma, West Chester, OH). The relative plasmin concentration was measured at an absorbance of 405 nm using a BioTek ELx808 plate reader²⁶⁻²⁸.

Evans blue (EB) assay

Mice received a single tail vein injection of 40 mg/kg EB (Thermo Fisher Scientific) in 50 μ L normal saline and were extensively perfused via intracardiac puncture 3 h later. Brain and lung tissue were homogenized and extracted in formamide and centrifuged (5,000 x g for 30 min). Optical density of the supernatant was measured at 620 nm using a spectrophotometer

²⁹.

***In vivo* quantification of aortic endothelial surface ANXA2³⁰**

Before the thoracic aorta was harvested, the animal was perfused via the left ventricle with 10 mL of ice-cold PBS at 2 mL/min, followed by 5 ml cell-impermeable sulfo-NHS-SS-biotin (1 mg/ml) at 1 mL/min⁻¹. Excess biotin was then quenched by infusion of 5 mL 50 mmol/LNH₄Cl. Cell surface biotinylated proteins were streptavidin (agarose-conjugated) precipitated from equal protein concentrations of aortic homogenate and analyzed by Western immunoblotting with anti-ANXA2 mAb. In the experiments studying aortic endothelial surface level of ANXA2 in rANXA2- or BSA-treated mice, carotid arteries were exposed to FeCl₃ before the animals were perfused with sulfo-NHS-SS-biotin.

Lipid rafts extraction and analysis

Detergent-insoluble cell lysate fractions were extracted on discontinuous sucrose gradients³¹. Briefly, cells were washed twice in ice-cold PBS, harvested, resuspended in 1 ml MES-buffered saline /Triton X-100 buffer (25mmol/L 2-[N-morpholino] ethanesulfonic acid 4-morpholineethane sulfonic acid, 150 mmol/L NaCl, pH 6.0, 1% Triton X-100, and

Protease Inhibitor Cocktail] and incubated on ice for 30 min. The cells were then lysed by passage through a 23 g needle ten times followed by sonic pulses using a sonicator (Thermo Fisher Scientific). Lysates were centrifuged at 800 x g for 10 min. The resulting supernatants (postnuclear fractions) were collected and transferred to separate tubes. One mL of sample was mixed with 1 mL of 90% sucrose/MBS solution and overlaid using 2 mL 35% sucrose in MBS/Triton X-100 buffer, and then 1 mL 5% sucrose in MBS/Triton X-100 buffer. Samples were centrifuged at 260,000 x g at 4 °C for 19 h and fractionated from the top (0.5 mL each for a total of ten fractions). Fractions were used immediately for assay or kept frozen at -80° C until analysis.

For lipid raft-associated monosialotetrahexosyl ganglioside (GM1; a marker of lipid rafts) assays, GM1 in detergent-insoluble fractions collected from sucrose gradients was studied by dot blot analysis to verify lipid raft fractions from the cell membrane³¹. Briefly, 1 µl of each fraction was spotted directly on to a nitrocellulose membrane. The membrane was dried for 5 minutes and blocked with 5% bovine serum albumin in PBS-0.1% Tween 20 (vol/vol) for 1 h at room temperature, and incubated with CTB-HRP (10 µg/L; Sigma Aldrich). GM1 was visualized using an enhanced chemiluminescence kit (LI-COR Biosciences). In order to verify non-lipid raft fractions from cell membrane, immunoblotting with anti-transferrin receptor (TfR) (non-lipid raft in cell membrane marker) antibody (1:1,000) was performed. Equal amounts of total protein from TfR-free lipid raft fractions and non-lipid raft fractions were analyzed by immunoblotting with anti-ANXA2 mouse monoclonal and anti-S100A10. To analyze the size of lipid rafts, HUVECs were stained with FITC-labeled CTB subunit (Sigma Aldrich) and incubated for 30 minutes at 37°C, and absorbance was measured at 495 nm with a Thermo Fluoroskan microplate reader. The amount of cholesterol and phospholipid in purified lipid rafts was assayed using the Amplex Red Cholesterol Assay Kit (Invitrogen) and EnzyChrom Phospholipid Assay Kit (BioAssay Systems) according to manufacturer's protocols, respectively. The absorbance was measured with a Thermo Fluoroskan microplate reader at a single excitation 530 nm, and cholesterol/phospholipid values were normalized to the protein concentrations. All experiments were repeated three times.

Real-time quantitative polymerase chain reaction (qRT-PCR)

Total RNA was prepared from tissue or cell samples using the TRIzol (Life Technologies). Total RNA was quantitated using NANO Drop 2000 (Thermo Fisher Scientific). Complementary DNA was prepared with iScript Reverse Transcription Supermix for qRT-PCR (Bio-Rad, Hercules, CA), and qRT-PCR was carried out with primers for ANXA2 (Fwd: 5'-CAA CTT TGA TGC TGA GCG GGA TG-3' and Rev: 5'-TGA CAA TGG CCT CGT CCA CAC-3') and S100A10 (Fwd: 5'-AGA TGG CAA AGT GGG CTT CC-3' and Rev: 5'-GGG ACA ACT CTT ATC AGG GAG GAG-3'), and iTaq Universal SYBR Green PCR Supermix (Bio-Rad). We normalized both mouse and human data using housekeeping genes, actin and glyceraldehyde-3-phosphate dehydrogenase (GAPDH), as references.

Statistics

Statistical significance was determined using Student's t-test or one-way analysis of variance. Results were regarded as significant if two-tailed P values were < 0.05 . All data are expressed as mean \pm standard error of the mean.

References

1. Gong B, Lee YS, Lee I, et al. Compartmentalized, functional role of angiogenin during spotted fever group rickettsia-induced endothelial barrier dysfunction: evidence of possible mediation by host tRNA-derived small noncoding RNAs. *BMC Infect Dis*. 2013;13:285.
2. Kopperud RK, Rygh CB, Karlsen TV, et al. Increased microvascular permeability in mice lacking Epac1 (Rapgef3). *Acta Physiol (Oxf)*. 2016.
3. Yan J, Mei FC, Cheng H, et al. Enhanced leptin sensitivity, reduced adiposity, and improved glucose homeostasis in mice lacking exchange protein directly activated by cyclic AMP isoform 1. *Mol Cell Biol*. 2013;33(5):918-926.
4. Gong B, Shelite T, Mei FC, et al. Exchange protein directly activated by cAMP plays a critical role in bacterial invasion during fatal rickettsioses. *Proc Natl Acad Sci U S A*. 2013;110(48):19615-19620.
5. Weiler-Guettler H, Christie PD, Beeler DL, et al. A targeted point mutation in thrombomodulin generates viable mice with a prethrombotic state. *J Clin Invest*. 1998;101(9):1983-1991.
6. Park SY, Yang JS, Schmider AB, Soberman RJ, Hsu VW. Coordinated regulation of bidirectional COPI transport at the Golgi by CDC42. *Nature*. 2015;521(7553):529-532.
7. Ling Q, Jacovina AT, Deora A, et al. Annexin II regulates fibrin homeostasis and neoangiogenesis in vivo. *J Clin Invest*. 2004;113(1):38-48.
8. Ishii H, Yoshida M, Hiraoka M, et al. Recombinant annexin II modulates impaired fibrinolytic activity in vitro and in rat carotid artery. *Circ Res*. 2001;89(12):1240-1245.
9. Li W, McIntyre TM, Silverstein RL. Ferric chloride-induced murine carotid arterial injury: A model of redox pathology. *Redox Biol*. 2013;1:50-55.
10. Konstantinides S, Schäfer K, Thinnies T, Loskutoff DJ. Plasminogen activator inhibitor-1 and its cofactor vitronectin stabilize arterial thrombi after vascular injury in mice. *Circulation*. 2001;103(4):576-583.
11. Gong B, Trent MB, Srivastava D, Boor PJ. Chemical-induced, nonlethal, developmental model of dissecting aortic aneurysm. *Birth Defects Res A Clin Mol Teratol*. 2006;76(1):29-38.

12. Lu B, Su Y, Das S, et al. Peptide neurotransmitters activate a cation channel complex of NALCN and UNC-80. *Nature*. 2009;457(7230):741-744.
13. Surette AP, Madureira PA, Phipps KD, Miller VA, Svenningsson P, Waisman DM. Regulation of fibrinolysis by S100A10 in vivo. *Blood*. 2011;118(11):3172-3181.
14. Smith AA, Jacobson LJ, Miller BI, Hathaway WE, Manco-Johnson MJ. A new euglobulin clot lysis assay for global fibrinolysis. *Thromb Res*. 2003;112(5-6):329-337.
15. Jirouskova M, Shet AS, Johnson GJ. A guide to murine platelet structure, function, assays, and genetic alterations. *J Thromb Haemost*. 2007;5(4):661-669.
16. Wolff B, Zsak M, Rabeck C. Immunofluorescence assay for the quantitative and qualitative evaluation of intracellular interleukin-8 in microtiter plates. *Anal Biochem*. 1997;244(1):33-39.
17. Friis T, Kjaer Sørensen B, Engel AM, Rygaard J, Houen G. A quantitative ELISA-based co-culture angiogenesis and cell proliferation assay. *APMIS*. 2003;111(6):658-668.
18. Hijazi N, Abu Fanne R, Abramovitch R, et al. Endogenous plasminogen activators mediate progressive intracerebral hemorrhage after traumatic brain injury in mice. *Blood*. 2015;125(16):2558-2567.
19. Mostowy S, Janel S, Forestier C, et al. A role for septins in the interaction between the *Listeria monocytogenes* INVASION PROTEIN InlB and the Met receptor. *Biophys J*. 2011;100(8):1949-1959.
20. Gong B, Ma L, Liu Y, et al. Rickettsiae induce microvascular hyperpermeability via phosphorylation of VE-cadherins: evidence from atomic force microscopy and biochemical studies. *PLoS Negl Trop Dis*. 2012;6(6):e1699.
21. Mostowy S, Janel S, Forestier C, et al. A role for septins in the interaction between the *Listeria monocytogenes* INVASION PROTEIN InlB and the Met receptor. *Biophys J*. 2011;100(8):1949-1959.
22. Xie H, Yin M, Rong W, Sun L. In situ quantification of living cell adhesion forces: single cell force spectroscopy with a nanotweezer. *Langmuir*. 2014;30(10):2952-2959.
23. Hermanowicz P, Sarna M, Burda K, Gabryś H. AtomicJ: an open source software for analysis of force curves. *Rev Sci Instrum*. 2014;85(6):063703.
24. Ellis V, Whawell SA. Vascular smooth muscle cells potentiate plasmin generation by both urokinase and tissue plasminogen activator-dependent mechanisms: evidence for a specific tissue-type plasminogen activator receptor on these cells. *Blood*. 1997;90(6):2312-2322.
25. O'Connell PA, Surette AP, Liwski RS, Svenningsson P, Waisman DM. S100A10 regulates plasminogen-dependent macrophage invasion. *Blood*. 2010;116(7):1136-1146.
26. Yavlovich A, Higazi AA, Rottem S. Plasminogen binding and activation by *Mycoplasma fermentans*. *Infect Immun*. 2001;69(4):1977-1982.
27. Siemens N, Patenge N, Otto J, Fiedler T, Kreikemeyer B. *Streptococcus pyogenes* M49 plasminogen/plasmin binding facilitates keratinocyte invasion via integrin-integrin-linked kinase (ILK) pathways and protects from macrophage killing. *J Biol Chem*. 2011;286(24):21612-21622.
28. Mundodi V, Kucknoor AS, Alderete JF. Immunogenic and plasminogen-binding surface-associated alpha-enolase of *Trichomonas vaginalis*. *Infect Immun*. 2008;76(2):523-531.
29. Luo M, Flood EC, Almeida D, et al. Annexin A2 supports pulmonary microvascular integrity by linking vascular endothelial cadherin and protein tyrosine phosphatases. *J Exp Med*. 2017.
30. Deora AB, Kreitzer G, Jacovina AT, Hajjar KA. An annexin 2 phosphorylation switch mediates p11-dependent translocation of annexin 2 to the cell surface. *J Biol Chem*. 2004;279(42):43411-43418.
31. Abbal C, Lambelet M, Bertaggia D, et al. Lipid raft adhesion receptors and Syk regulate selectin-dependent rolling under flow conditions. *Blood*. 2006;108(10):3352-3359.
32. Wei Y, Li K, Wang N, et al. Activation of endogenous anti-inflammatory mediator cyclic AMP attenuates acute pyelonephritis in mice induced by uropathogenic *Escherichia coli*. *Am J Pathol*. 2015;185(2):472-484.
33. Díaz-Ramos A, Roig-Borrellas A, García-Melero A, López-Aleman R. α -Enolase, a multifunctional protein: its role on pathophysiological situations. *J Biomed Biotechnol*. 2012;2012:156795.

34. Jalkanen S, Karikoski M, Mercier N, et al. The oxidase activity of vascular adhesion protein-1 (VAP-1) induces endothelial E- and P-selectins and leukocyte binding. *Blood*. 2007;110(6):1864-1870.

Supplementary figure legends

Fig. S1: Generation of EPAC1-null mice. Genomic organization of the wild-type allele and mutant alleles for the *EPAC1* (also known as *Rapgef3*) gene (A). Western immunoblotting (B) shows normal EPAC1 expression in wild-type (+/+) mice lung, kidney, and brain, compared to no EPAC1 detected in *EPAC1*-null (-/-) mice. There is also no difference of ANXA2 and S100A10 expression in lung, kidney, and brain between wild-type and *EPAC1*-null mice.

Fig.S1

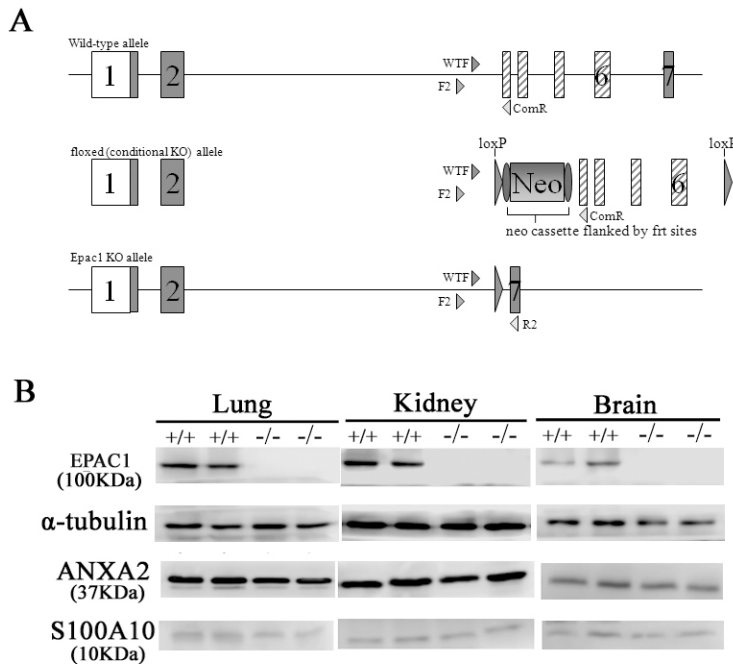
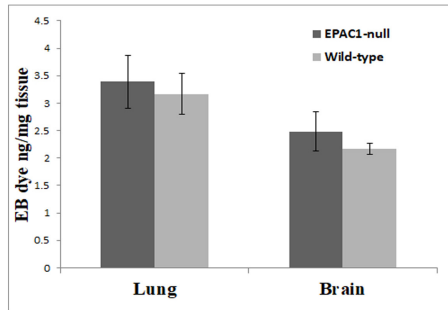


Fig. S2: Vascular integrity assessments. Evans blue (EB) assay revealed no difference in the baseline of extravascular dye in brain and lung parenchyma (A); immunofluorescent microscopy (IF) analysis (B) displayed similar structures of vascular tight (red) or adherens junctions (red) between wild-type (n=6) and *EPAC1*-null (n=6) mice. Normal rabbit serum (Fig. S3) or mouse IgG were used as antibody controls during IF. Scale bars indicate 20 μ m.

Fig.S2

A



B

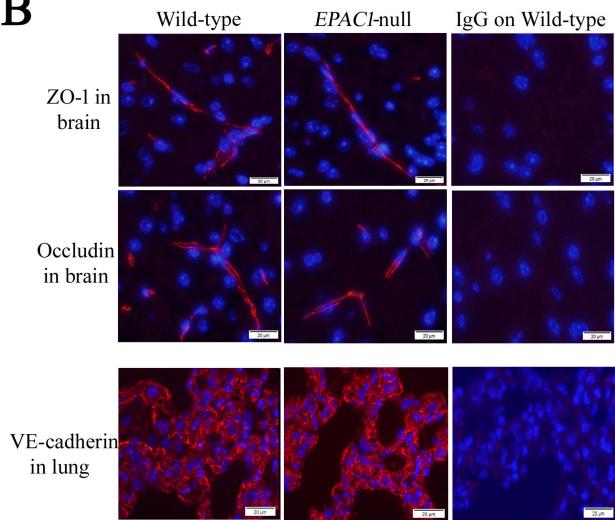


Fig. S3: Normal rabbit serum was used as an antibody control during IHC or IF. Scale bars indicate 50 μm in IHC and 20 μm in IF.

Fig.S3

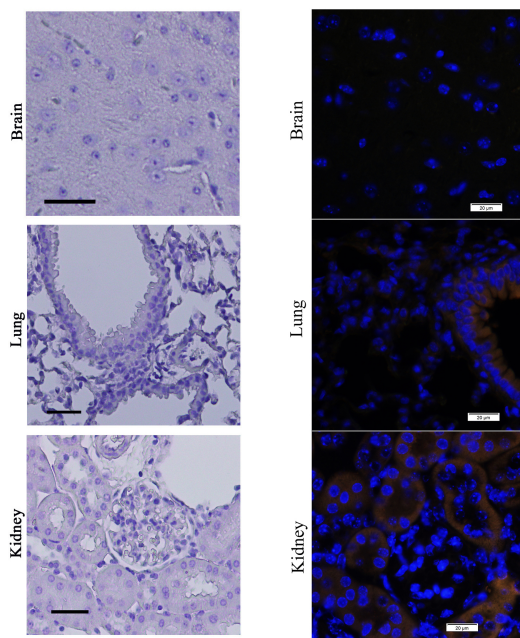


Fig.S4

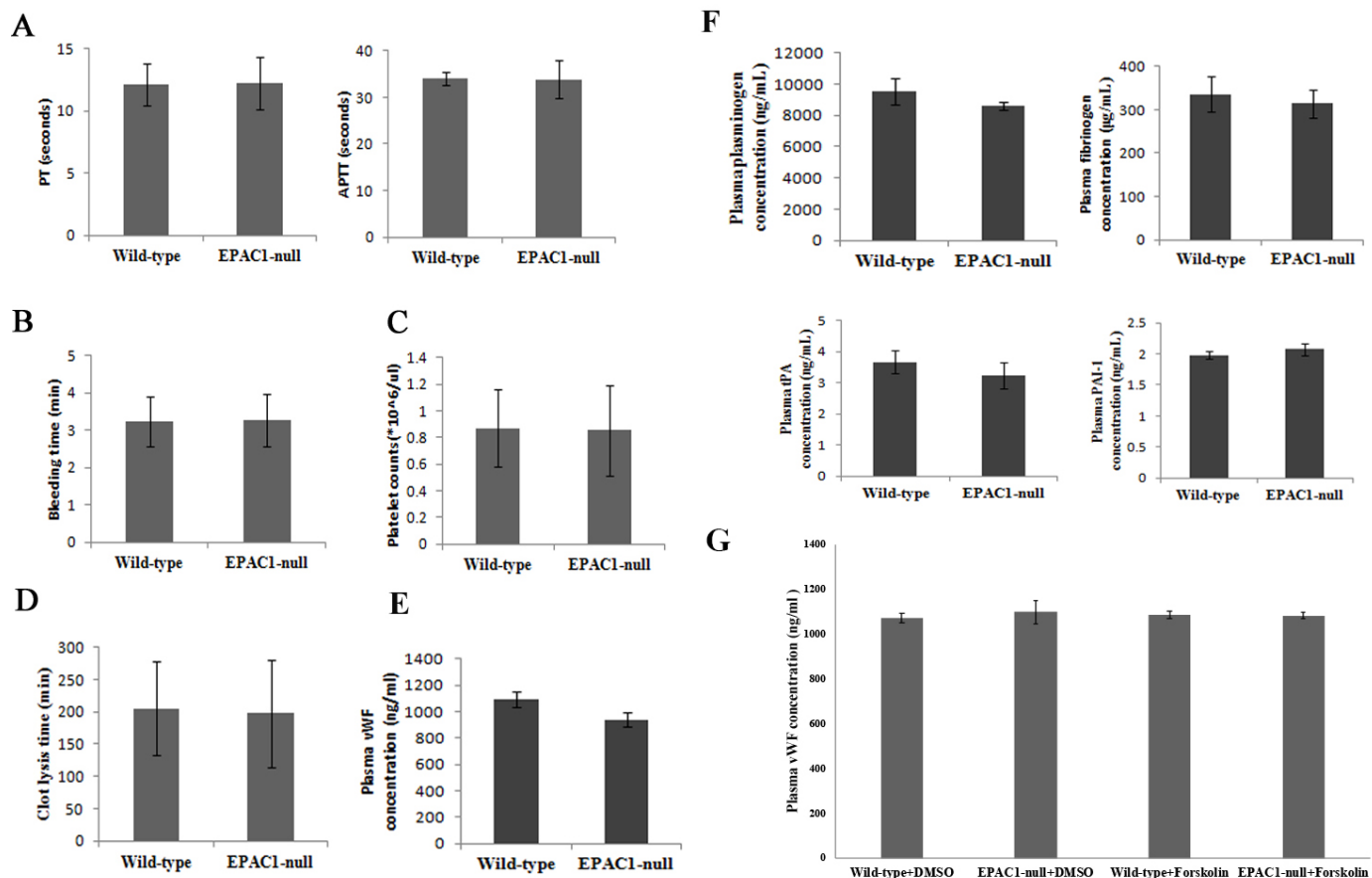


Fig. S4: Comparison of clotting parameters and other components of the fibrinolytic system. There are no statistically significant differences in the prothrombin time (PT), activated partial thromboplastin time (aPTT), platelet count, bleeding time, clot lysis time, and plasma levels of vWF between wild-type (n=10) and *EPAC1*-null (n=10) mice. There are no differences in the plasma levels of plasminogen, fibrinogen, tPA, and plasminogen activator inhibitor-1(PAI-1) between wild-type (n=10) and *EPAC1*-null (n=10) mice. To rule out potential effect from cAMP activator on the level of vWF secretion in vivo, wild-type (n=6) and *EPAC1*-null (n=6) mice were treated with forskolin (10 mg/kg)³² intraperitoneally 1 hour before euthanasia for blood collection. Six mice (three wild-type and three *EPAC1*-null) of the control group were treated with vehicle.

Fig. S5: Histological observation of FeCl₃-induced carotid arterial thrombosis. Representative hematoxylin and eosin staining was employed to detect FeCl₃-induced carotid arterial thrombus (T) in *EPAC1*-null (A), wild-type (B), *EPAC1*-null pretreated with BSA (C), and *EPAC1*-null pretreated with rANXA2 (D) mice. Scale bars indicate 20 μ m.

Fig.S5

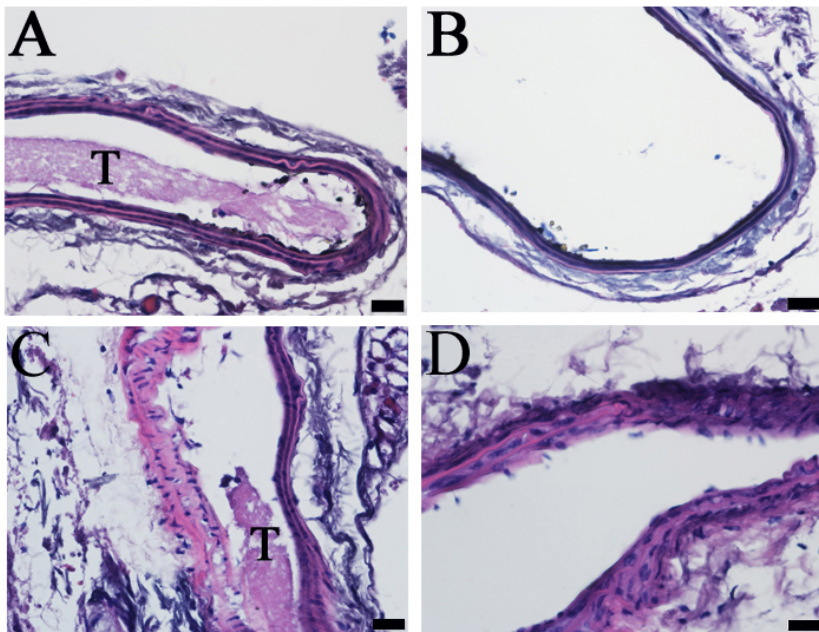


Fig. S6: Absence or inhibition of EPAC1 does not affect *de novo* protein synthesis of ANXA2 and S100A10. Western immunoblotting shows no difference of ANXA2 and S100A10 expression in lung, kidney, and brain between wild-type and *EPAC-null* mice (Fig.S1B). qRT-PCR (B) shows no difference in ANXA2 and S100A10 mRNA levels in lung, kidney, and brain from wild-type and *Epac-null* mice (A). Western immunoblotting shows no difference of ANXA2 and S100A10 expression in ESI09-treated HUVECs compared with vehicle-treated HUVECs (B). qRT-PCR (B) shows no difference of ANXA2 and S100A10 in mRNA levels in ESI09-treated HUVECs compared with vehicle-treated HUVECs (C).

Fig.S6

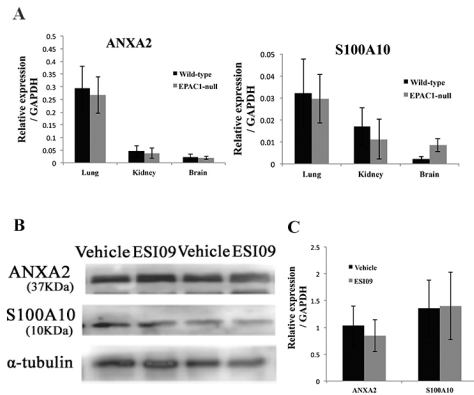


Fig. S7: Lipid raft fraction-associated monosialotetrahexosyl ganglioside assay and non-lipid raft fraction-associated immunoblotting with anti-transferrin receptor. These two assays verify both lipid raft fractions (samples 2-4) and non-lipid raft fractions (samples 7, 9, and 10) from HUVEC membrane fractionations as described in the Method and Materials section (A). The amounts of cholesterol, phospholipid, and GM1 in purified lipid rafts were measured and there were no significant differences between vehicle- and ESI09-treated HUVECs (B).

Fig.S7

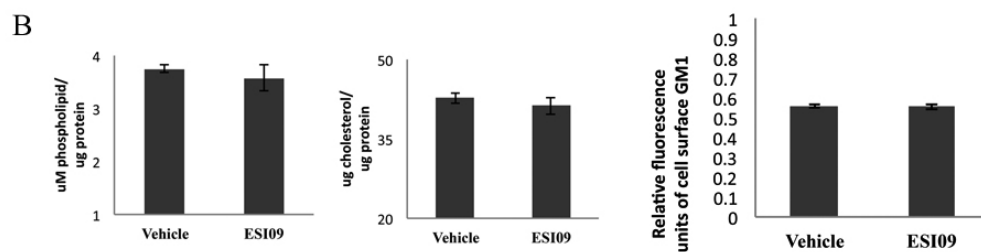
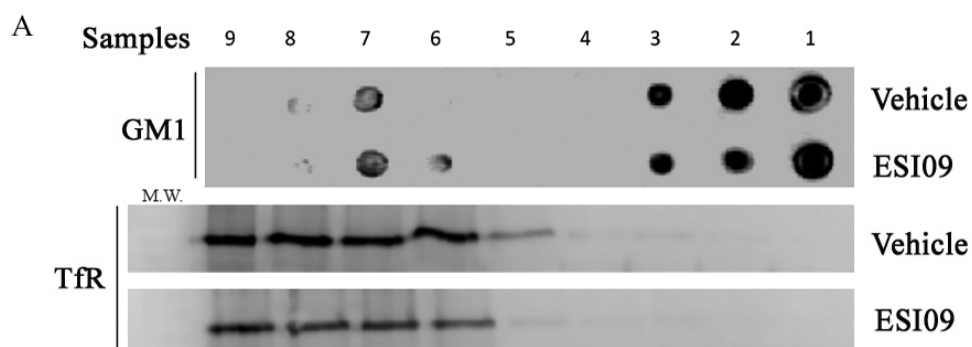


Fig. S8: Comparison of other plasminogen receptors³³ on the endothelial cell surface. There are no differences in impermeable cell-based ELISA assays of enolase, plasminogen receptor-KT (PLGRKT), and cytokeratin 8 between vehicle- (n=6) and ESI09-treated (n=6) HUVECs.

Fig.S8

